RSC Advances

PAPER

View Article Online
View Journal | View Issue

Cite this: *RSC Adv.*, 2020, **10**, 4561

PEGylated gold nanorods with a broad absorption band in the first near-infrared window for *in vivo* multifunctional photoacoustic imaging†

Yiping Wang,[a] Yiduo Wu,[a] Qiang Wen,[a] Pengwei Li,*[a] Ying Wang,[b] Huabei Jiang[c] and Wendong Zhang[a]

Received 12th December 2019
Accepted 16th January 2020

DOI: 10.1039/c9ra10442a

rsc.li/rsc-advances

Nanoparticles with absorbances in the near-infrared window (NIR, 700–1300 nm) are ideal contrast agents for *in vivo* imaging of deep tissue with high signal-to-noise ratios. By using CTAB and L(+)-ascorbic acid (AA) as ligands to effectively balance particle nucleation and growth, PEGylated Au nanorods (NRs) with broad absorption bands (from 650 to 1100 nm) in the first NIR window could be successfully realized. The morphologies, crystal structures, absorption and biotoxicities of the samples were determined by TEM, TGA, UV-vis and MTT assay. The results indicated that the presence of a thin poly(ethylene glycol) (PEG) shell could greatly improve the biocompatibility of the Au NRs (1.7 times that of non-PEGylated Au NRs), making them harmless to living cells. Moreover, the prepared PEGylated Au NRs displayed the highest image contrast and SNR values (1.1–1.5 times that of commercial Au nanospheres and NRs), with excitation lasers of 532, 680 and 828 nm, showing their great potential for use in multicolor photoacoustic imaging *in vivo*. With the prepared PEGylated Au NRs, a functional image of oxygen saturation was constructed in a single step without changing the contrast agent.

1 Introduction

Near-infrared (NIR) light penetrates deep into the body and is subject to minimal interference from the scattering, absorption and autofluorescence of tissue and blood, which makes it favorable for *in vivo* photoacoustic imaging (PAI) and photothermal therapy (PTT).[1–4] In particular, light within the two transparent biological windows, located at 650–950 nm (NIR-I window) and 1000–1350 nm (NIR-II window), can image deep tissue with high signal-to-noise ratios (SNRs).[5–8] Nanoparticles, especially those with strong absorption in the NIR region, are promising labels for exogenous PAI and PTT agents due to their unique optical properties.[9–13] However, most of the studied nanoparticles, such as small-molecule dyes,[14] semiconductors,[15–17] upconversion nanoparticles,[18,19] carbon-based nanotubes and rGO,[20–22] have low thermal stabilities or exhibit some degree of biotoxicity, which limits their *in vivo* applications.

Au nanoparticles, which have excellent chemical stabilities, low biotoxicities and tunable absorbance bands in the NIR region, have been reported as promising contrast agents for NIR PAI and PTT.[23–28] Au nanoparticles designed with a rod-in-shell structure and tailored to be responsive in the first and second NIR windows have been prepared and applied for hyperthermia-based therapy.[29] Likewise, gold nanostars have also been successfully synthesized, with greater than 320-fold fluorescence enhancement in the first NIR-I window and 50-fold enhancement in the NIR-II region.[30] In addition, gold nanorods (with an aspect ratio of approximately 3.5) emitting at approximately 700 nm have been prepared and used as contrast agents in a combined PA/Raman imaging system for the detection of ovarian cancer.[31] Biodegradable gold nanovesicles with an ultrastrong plasmonic coupling effect have also been successfully synthesized and applied to PAI and PTT.[32] However, it is still a challenge to tune the bandwidth of the emission of Au nanoparticles in the NIR region,[33–35] which is necessary for realizing multicolor labeling to synchronously image multiple targets with high SNRs.[36] For instance, multifunctional PAI of oxygen saturation requires at least two different wavelength lasers for synchronous image.[37]

Herein, we report a seed-assistant method to synthesize Au nanorods (NRs) with a broad absorption band ranging from 650 nm to 1100 nm or greater. The synthesized Au NRs were modified with thiolated poly(ethylene glycol) (thiol-PEG) and utilized in PAI. The results reveal that the sample has low cytotoxicity and can achieve excellent imaging efficacy of the

[a]*Micro-Nano System Research Center, College of Information and Computer, Taiyuan University of Technology, Taiyuan 030024, Shanxi, China. E-mail: lipengwei@tyut.edu.cn*

[b]*College of Mechanics, Taiyuan University of Technology, Taiyuan 030024, Shanxi, China*

[c]*Biomedical Optics Laboratory, Department of Medical Engineering, College of Engineering, University of South Florida, Tampa, FL 33620, USA*

† Electronic supplementary information (ESI) available. See DOI: 10.1039/c9ra10442a

blood vessels in mouse brain. The obtained multicolor PA images were analyzed to probe the metabolism *in vivo* and pixel-by-pixel calculations allowed multifunctional PA images of oxygen saturation to be obtained.

2 Experimental section

2.1 Synthesis of Au nanorods

Au NRs were synthesized by a modified seed-mediated synthetic method.[38,39] In a typical procedure (Scheme 1), 10.3 mL of 0.025 M $HAuCl_4$ (Sinopharm Chemical Reagent Co., Ltd., ≥99.9%) and 1.823 g of cetyl trimethyl ammonium bromide (CTAB) surfactant (Tianjin Guangfu Fine Chemical Research Institute, ≥99.0%) were first added to a beaker. Then, deionized water (18 MΩ) was added to bring the total concentration of $HAuCl_4$ to be 2.5×10^{-3} M, and CTAB of 0.05 M. Four flasks tagged as A, B, C and D, were separately transferred into 10 mL, 4.5 mL, 4.5 mL and 45 mL of the above-mentioned solution in proper order. Then, 350 μL of 0.01 M ice-cold $NaBH_4$ (Sinopharm Chemical Reagent Co., Ltd, ≥98.0%) was added to flask A, and stirred for 6.5 min. 0.4 mL of solution in flask A and 25 μL of 0.1 M L(+)-ascorbic acid (AA) (Tianjin Shentai Chemical Industry Co., Ltd., ≥99.7%) were transferred into flask B, and the solution was stirred for 3 min. And then, 0.4 mL of solution in flask B and 25 μL of 0.1 M AA were added to flask C, stirred for 3 min again. Finally, 4 mL solution of flask C and 250 μL of 0.1 M AA were added to flask D, stirred for 5 s and left undisturbed in a water bath at 28 °C for 12 h, until the reaction completed. The top layer of the solution was carefully removed, and 10 mL of deionized water was added to disperse the precipitate; the solution was centrifuged, and washed several times with distilled water to fully remove excess CTAB.

2.2 Surface modification of the Au nanorods

First, 10 mg of thiol-PEG (Nanjing Pengsheng Biological Technology Co. Ltd) was dissolved in 1 mL of deionized water and sonicated for 10 min. Then, the solution was treated with 50 mL of a 0.1 M $NaBH_4$ solution under sonication for another 15 min to prevent the possible dimerization of thiol-PEG (PEG-S-S-PEG). Second, the washed Au nanorods were dispersed in 10 mL of deionized water, mixed with the above thiol-PEG solution (10 mL) *via* stirring for 5 min and then left undisturbed for 5 h. Finally, the sample was centrifuged several times for 10 min at 3500 rpm and dispersed in 4 mL of deionized water for further application.

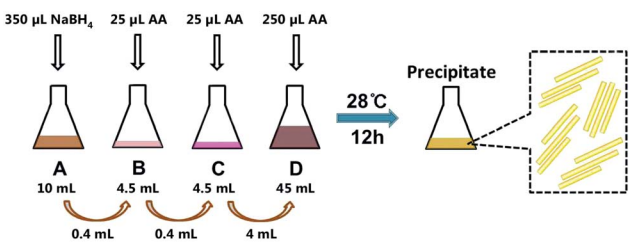

Scheme 1 Scheme for the synthesis of Au nanocrystals.

2.3 Characterization

The morphologies and structures of the as-synthesized Au nanorods were identified by transmission electron microscopy (TEM, JEOL 2100F, 200 kV). UV-vis absorbances of the various Au nanorods were identified by spectrophotometry (Shimadzu, 3100 UV-vis-NIR). TGA analysis was performed on NETZSCH (STA-409-pc) using a heating rate of 20 °C min^{-1} up to 700 °C under N_2 condition. The PA signals were recorded and normalized by a unit rotation scanning PA detection system (Fig. S1†), which contained a laser (Surelite I-20, Continuum), an optical parametric oscillator (OPO, Surelite OPO Plus), a nonfocused ultrasonic transducer (PMUT, V310-SU, Olympus, 5 MHz), a stepper motor rotating table and motor control box (MC, M600, Beijing Zhuo Li Han Guang Instrument Co., Ltd.), preamplifier (5077 PR, Olympus), and a PCI4732 data acquisition (DAQ) card. A 532 nm laser beam was directly emitted from the laser, and further laser wavelengths were obtained *via* the OPO.

2.4 Cell viability experiments

All bio-experimental procedures were approved by IACUC committee at Taiyuan University of Technology. And the experiments were carried out in accordance with the approved guidelines. HeLa cells were cultured in the standard cell medium recommended by the American Type Culture Collection (ATCC) at 37 °C under a 5% CO_2 atmosphere. Cells were seeded into 96-well plates and incubated with different concentrations of Au nanoparticles (Au NRs, Au NR@PEG, and commercial Au nanospheres and Au NRs) for 24 h. The relative cell viabilities were determined by a standard methyl thiazolyl tetrazolium (MTT) assay and imaged *via* an optical microscope.

2.5 *In vitro* and *in vivo* photoacoustic imaging

The Au NR@PEG (1 nM) solutions were irradiated under 828 nm excitation at a power density of 15 mJ cm^{-2} for 30 min (laser on), then by natural cooling at room temperature without laser irradiation (laser off). This cycle was repeated five times and the UV-vis spectra of the samples were obtained to characterize the photostability of their absorption properties. Agar powder (2 g, Gene Company Ltd.) was dissolved in a beaker in 100 mL of deionized water and mixed well with a glass rod. The turbid liquid was heated to boiling in a microwave oven (Midea Group Co., Ltd.). Then, the liquid was removed and stirred in a water bath for 20 min at 60 °C until the liquid thickened. Then, the viscous material was poured into a 4.5 cm diameter cylindrical mold, cooled and solidified. Finally, the solid agar was used as a biological tissue phantom due to its absorbance of NIR excitation approximating that of biological systems.

A 0.9 mm diameter glass capillary, which could be filled with fresh ox blood or blood mixed with various concentrations of Au NR@PEG in specific experiments, was implanted into the surface of the phantom to simulate blood vessels. The phantom

was placed under water and irradiated with a 680 nm or 828 nm laser at a power density of 15 mJ cm^{-2} (Fig. S2†).

The mouse was transiently narcotized with isoflurane, then 0.04 mL/10 g of 10 wt% chloral hydrate was intraperitoneally injected to ensure the mouse was thoroughly anesthetized. The mouse head was gently shaved of hair and smoothly coated with an ultrasonic coupling agent (Boline Healthcare Ltd). The wavelength of the laser was adjusted to 828 nm, and the mouse was placed under water. Then, the cerebral blood vessels of the mouse were imaged before and after intravenously (IV) injecting the contrast agents (Au NR@PEG, commercial Au nanospheres and Au nanorods; 1 nM solutions, 0.1 mL/10 g body weight). The laser excitation was changed to 680 and 532 nm, and the above experiment was repeated. Notably, when the contrast agent was changed, subsequent IV injection should occur at least 24 h later to allow the residual contrast agent to be completely metabolized.

3 Results and discussion

The typical morphologies and structures of the three different Au nanostructures were initially determined by scanning electron microscopy (SEM) and UV-vis (Fig. 1). Fig. 1a shows the typical morphology of the synthesized Au NRs, which had diameters of approximately 22 nm and aspect ratios ranging from 6 to 18. The commercial Au nanospheres had a diameter of 25 ± 5 nm and are shown in Fig. 1b. Fig. 1c presents the typical shape of the commercial Au nanorods, which had a diameter of approximately 10 nm and lengths of 33 ± 7 nm. The absorption spectra of the samples were determined by UV-vis (Fig. 1d). Compared with the commercial Au nanospheres (absorption peak at approximately 520 nm) and nanorods (absorption peaks at 520 and 800 nm), the synthesized Au NRs exhibit a broad absorption band (ranging from 650 to 1100 nm) over the first NIR window (650–950 nm),[7] indicating their potential widespread use in NIR imaging in the medical field. It is suspected that this broadening of the longitudinal surface plasmon resonance (SPR) band is dominated by differences in the aspect ratios of different Au nanorods.[40,41]

The prepared Au NRs can be conveniently transferred to the aqueous phase for PEGylation, as shown schematically in Fig. 2. Fig. 2a is a brightfield TEM image, which shows the typical rod-like characteristics of the sample. Fig. 2b displays the UV-vis absorption spectra of the synthesized Au NRs before and after being PEGylated. Though they have similar absorption features, the PEGylated Au NRs exhibit a 16.5 nm redshift of the absorption peak. This redshift may be ascribed to the thin PEG shell coating the Au NRs (Fig. 2c).TGA curve for Au NR@PEG evaluated by mass loss was recorded as a function of temperature (Fig. S3†). The total mass loss for Au NR@PEG was 35.3%, which indicated successful coating of PEG on the surface of Au NR. The selective area electron diffraction (SAED) pattern ([022] zone axis direction) in Fig. 2d reveals the cubic structure of the sample and demonstrates its good crystallinity. Fig. 2e shows the high-resolution TEM (HRTEM) image of the top surface of a single rod in area '1' highlighted by the red rectangle in Fig. 2c. The interplanar spacing was measured as 0.235 nm, corresponding to the Au {111} facet in the cubic phase.

The UV-vis spectra of Au NR@PEG showed no obvious decrease in the absorbance at 828 nm after five cycles of laser on/off (Fig. S4†). The result indicated that Au NR@PEG showed excellent photostability after a long period of laser irradiation. High absorption enhancement dominated the relatively weak background solvent spectrum in the NIR region for PAI.[6,10] Simulated blood vessels (Fig. 3a) were imaged separately at 532, 680 and 828 nm (Fig. 3b). From the PA images obtained under 532 nm excitation (Fig. 3b: b1, b4, b7 and b10), Au NR@PEG had a SNR almost equal to that of the commercial Au nanoparticles; when the laser wavelength was changed to 680 nm (Fig. 3b: b2, b5, b8 and b11), Au NR@PEG showed the highest image contrast of all four samples, and under 828 nm excitation (Fig. 3b: b3, b6, b9 and b12), Au NR@PEG was still one of the best contrast agents and provided the highest SNR. In

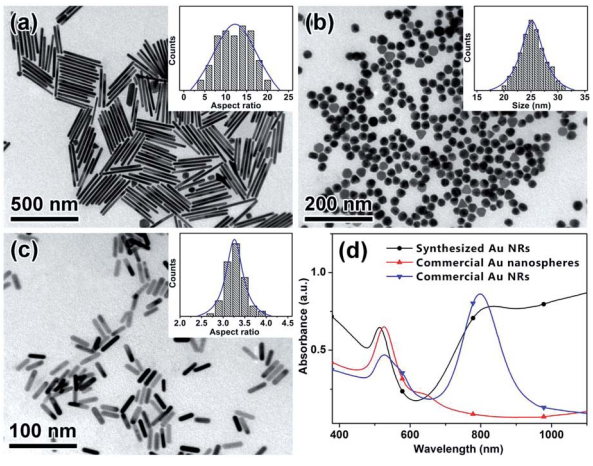

Fig. 1 Typical morphologies and absorption spectra of the Au nanoparticles. (a) The synthesized Au NRs with aspect ratios from 6 to 18; (b) commercial Au nanospheres with a diameter of approximately 25 nm; (c) commercial Au nanorods with an aspect ratio of approximately 3.3; and (d) absorption spectra of the three different Au nanocrystals.

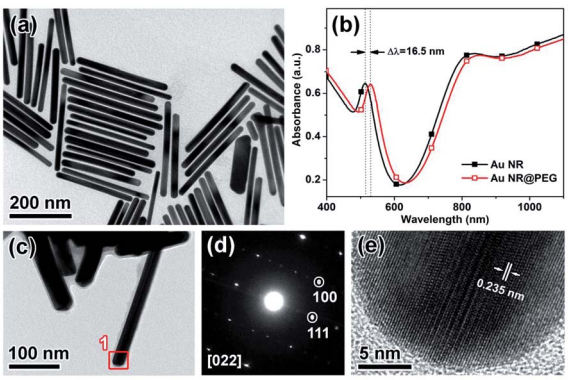

Fig. 2 Typical morphology and structure of the synthesized PEGylated Au NRs. (a) Brightfield TEM image; (b) UV-vis absorption spectra; (c) magnified TEM image; and (d and e) SAED pattern and HRTEM image of a single Au NR along the [022] zone axis.

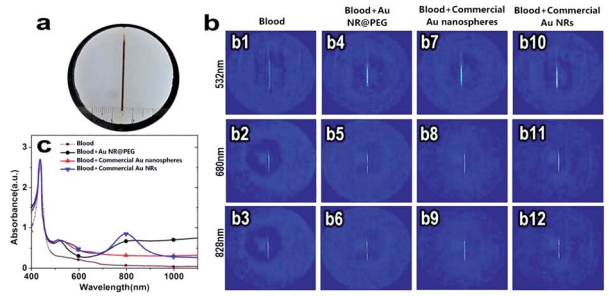

Fig. 3 (a) Photograph of a blood vessel simulated by implanting a 0.9 mm capillary glass tube into the agar phantom. The capillary glass tube was fulfilled with fresh ox blood. (b) PAI images of (a) obtained under different excitation wavelengths; (c) absorption spectrum of blood mixed with the three different contrast agents (1 nM).

summary, the synthesized Au NR@PEG exhibited promising multicolor PAI with high SNRs. The UV-vis absorption spectra of fresh ox blood and blood mixed with different concentrations of the PA contrast agents are shown in Fig. 3c, the results of which also reflect the enhancement of the PA effect by Au NR@PEG at different wavelengths, including approximately 532 nm and the broad NIR band from 650 to 1100 nm.

Additional *in vitro* PA properties of the PEGylated Au NRs are shown in Fig. 4, where Au NR@PEG was employed as a PAI contrast agent, mixed with fresh ox blood at different concentrations and illuminated with an 828 nm wavelength laser (Fig. 4a). The amplitudes of the PA signals demonstrate an obvious increase after Au NR@PEG had been added. The signal increase was nearly linear with respect to the concentration of Au NR@PEG from 0.25 to 1.0 nM (Fig. 4b). When the concentration reached 1 nM, the amplitude of the generated PA signal of the mixture was approximately 18.3 times higher than that of blood alone. The PA spectra and optical spectra of the three different Au nanocrystals (Au NR@PEG and commercial Au nanospheres and NRs) are shown in Fig. 4c–e. The

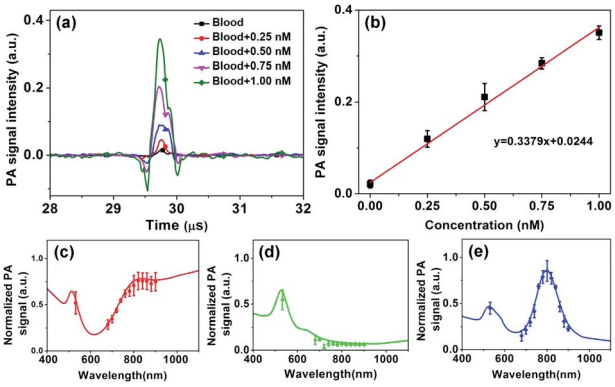

Fig. 4 (a) PA signals of Au NRs at various concentrations (from 0 to 1 nM), under 828 nm laser excitation; (d) linear fitting of the PA signal intensities for different concentrations of Au NRs; and (c–e) comparison of absorption spectra (solid line) of the synthesized and commercial Au nanoparticles obtained from multi-wavelength photoacoustic signals amplitude (data points).

multiwavelength PA spectra were obtained by collecting the intensities of the PA signals at different wavelengths (from 680 to 900 nm) when a 1 nM aqueous solution was added to the glass capillary tubes. Clearly, the PA spectra agree well with the absorption spectra of the samples, indicating that Au NR@PEG could provide excellent enhancement of the PA signal over a broad NIR region from 680 nm to 900 nm.

To examine the biotoxicity of the Au NRs for active targeting, HeLa cells were incubated with and without Au nanoparticles (Au NRs, Au NR@PEG and commercial Au nanospheres and NRs) at concentrations of 0.25–1.0 nM. A standard MTT assay was carried out to determine the viability of the cells (Fig. 5a). A plot and photographs of the dose-dependent cytotoxicity (Fig. 5a and S5†) show that most of the cells survived when cultured in the presence of Au NR@PEG, even at high concentrations of up to 1 nM (77.3%), compared with the survival of the other groups, after 24 h. This suggests that Au NR@PEG possess low cell cytotoxicity and good biocompatibility[42,43] and may be a promising PA contrast agent. Hematoxylin and eosin stained histological images (Fig. 5b) of four organs (heart, liver, kidney, and spleen) from mice treated with Au NR@PEG at 24 h postinjection show no appreciable abnormalities and show extremely low levels of residual Au nanoparticles in the body, which agrees well with the results above and indicates the relatively minimal effects of PEGylated Au NRs on biological organisms.

Appropriately applying contrast agents can increase the imaging depth and spatial resolution of *in vivo* PAI compared to those of traditional optical imaging methods.[6,44] Au NR@PEG, which provides a suitable absorption band in the NIR region and possesses low toxicity, was IV injected into a mouse (1 nM, 0.1 mL/10 g body weight) to obtain PA images in a living body (Fig. 6). The cerebral blood vessels of the mouse (Fig. 6a) were

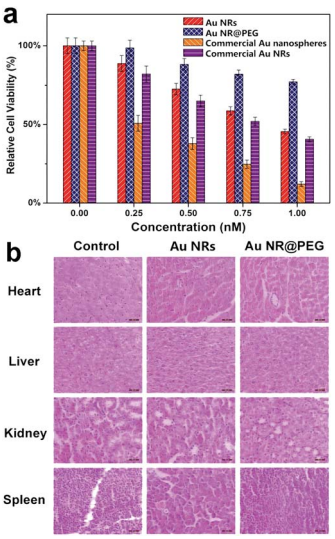

Fig. 5 (a) Relative viabilities of the cells *via* MTT assay after incubation with various concentrations of the different Au contrast agents for 24 h; (b) hematoxylin and eosin stained histological images of four organs (heart, liver, kidney, and spleen) from mice treated with Au NRs and Au NR@PEG after 24 h, scale bar: 50 μm.

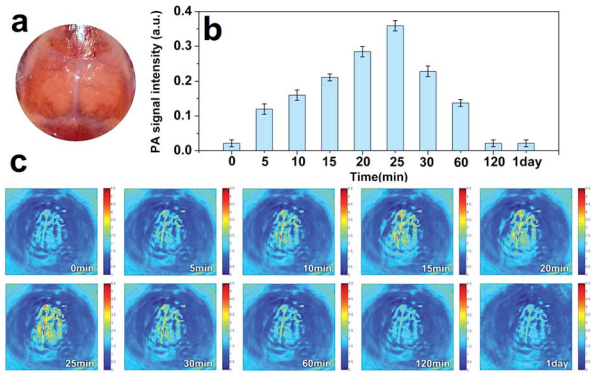

Fig. 6 (a) Images of mouse cerebral blood vessels; (b) relative PA signal intensity of the mouse cerebral blood vessels obtained at different time points after the injection of Au NR@PEG; (c) PA images of the mouse cerebral blood vessels after IV injection of Au NR@PEG under 828 nm laser excitation.

imaged with a PA system at several time points, ranging from 0 min to 1 day (Fig. 6b and c), under 828 nm laser irradiation. It is obvious that the PA signals were very weak and the blood vessels could barely be imaged at low contrast prior to Au NR@PEG being IV injected and metabolized over 2 h post-injection. Strong PA signals appeared after Au NR@PEG had been IV injected and reach a maximum at 25 min postinjection, indicating the efficient accumulation of the nanorods, likely owing to the enhanced permeability and retention (EPR) effect of living organisms.[19] The PA signal intensity returned to the initial value after 120 min, suggesting that Au NR@PEG was rapidly metabolized.

To verify the potential of Au NR@PEG for multicolor PAI, mouse was IV injected with the different Au nanocrystals (1 nM, 0.1 mL/10 g body weight) and imaged at different excitation wavelengths (532, 680 and 828 nm) with a power density of 15 mJ cm^{-2} (Fig. 7a).[34] Under 532 nm excitation, Au NR@PEG

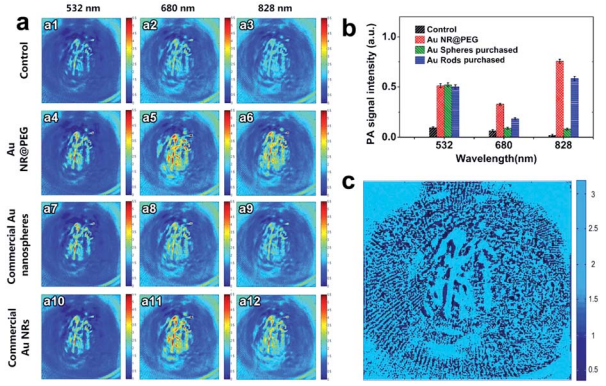

Fig. 7 (a) PA images of the mouse cerebral blood vessels obtained 25 min after IV injection of the three different contrast agents under different laser excitation wavelengths; (b) relative PA signal intensity obtained after injection of the three contrast agents under different laser excitation wavelengths; and (c) the calculated and reconstructed image of the blood oxygen concentration in the mouse cerebral blood vessels.

(Fig. 7: a4) exhibited contrast improvement equivalent to that of the commercial Au nanomaterials (Fig. 7: a7 and a10). Under 680 nm excitation, Au NR@PEG (Fig. 7: a5) and the commercial Au nanorods (Fig. 7: a11) showed the highest image contrast. When the laser wavelength was adjusted to 828 nm, Au NR@PEG (Fig. 7: a6) maintained the best image quality among the different contrast agents. In short, the prepared Au NR@PEG provided the best image enhancement at all the excitation wavelengths. These results are more obvious in the histogram of the relative PA signals (Fig. 7b). Image contrast (calculated from ten randomly selected points, which were at the same position for each PA image) and the SNR were also analyzed systemically to evaluate the image quality (Table 1). Compared with that of the control group, the image contrast of Au NR@PEG improved by 61.2% under 680 nm excitation and 80.0% under 828 nm excitation, which are largest enhancements among all of the samples. Likewise, the SNRs of the images of the Au NR@PEG group also greatly improved by 34.8%, 53.2% and 24.2% under 532 nm, 680 nm at 828 nm excitation, respectively.

Since the oxygenated hemoglobin and deoxygenated hemoglobin in biological tissue have different absorptivities to different laser wavelengths, the distribution of the blood oxygen concentration in the mouse cerebral blood vessels could be calculated and reconstructed according to the above results (Fig. 7c). We obtained the cerebral deoxyhemoglobin (Hb), oxyhemoglobin (HbO_2) and oxygen saturation (sO_2) values of the mouse cerebral blood vessels at two different excitation wavelengths (680 nm and 828 nm). The sO_2 changes were calculated pixel-by-pixel *via* the following equations, and the pixels were chosen according to the calculated total hemoglobin (HbT) concentration ($C_{HbT} = C_{HbO_2} + C_{Hb}$):[37]

$$sO_{2(x,y,z)} = \frac{C_{HbO_2(x,y,z)}}{C_{HbT(x,y,z)}} \quad (1)$$

$$\begin{pmatrix} C_{Hb} \\ C_{HbO} \end{pmatrix}_{(x,y,z)} = \left(\begin{bmatrix} \varepsilon_{Hb}(680) & \varepsilon_{HbO_2}(680) \\ \varepsilon_{Hb}(828) & \varepsilon_{HbO_2}(828) \end{bmatrix}^{T} \times \begin{bmatrix} \varepsilon_{Hb}(680) & \varepsilon_{HbO_2}(680) \\ \varepsilon_{Hb}(828) & \varepsilon_{HbO_2}(828) \end{bmatrix} \right)^{-1} \times \begin{bmatrix} \varepsilon_{Hb}(680) & \varepsilon_{HbO_2}(680) \\ \varepsilon_{Hb}(828) & \varepsilon_{HbO_2}(828) \end{bmatrix}^{T} \begin{pmatrix} \varphi_{680}(x,y,z) \\ \varphi_{828}(x,y,z) \end{pmatrix} k \quad (2)$$

where x and y represent the coordinates of pixels on the graph, z represents the intensity of each pixel or the total HbT concentration, C_{HbO_2} denotes oxygenated hemoglobin, and C_{Hb} refers to deoxygenated hemoglobin. All concentrations are with respect to total hemoglobin. Additionally, ε_{HbO_2} and ε_{Hb} represent the fixed molar extinction coefficients (cm^{-1} M^{-1}), which can be referred to as $\begin{bmatrix} \varepsilon_{Hb}(680) & \varepsilon_{HbO_2}(680) \\ \varepsilon_{Hb}(828) & \varepsilon_{HbO_2}(828) \end{bmatrix} = \begin{bmatrix} 2407.92 & 693.2 \\ 277.6 & 965.2 \end{bmatrix}$, φ_{680} and φ_{828} are the PA signal amplitudes acquired at the wavelengths of 680 nm and 828 nm, and k is the proportionality coefficient, which can be determined from the

Table 1 Contrast and SNRs of the PA images in Fig. 5. Contrast here is the mean value of the images of the mouse cerebral blood vessels; SNR denotes the signal–noise ratio determined from the whole image

	532 nm			680 nm			828 nm		
Conditions	Fig.	Contrast	SNR	Fig.	Contrast	SNR	Fig.	Contrast	SNR
Control	a1	3.182	0.9847	a2	2.475	0.4004	a3	1.912	0.2450
Au NR@PEG commercial	a4	4.763	1.3276	a5	3.989	0.6136	a6	3.442	0.3042
Au nanospheres	a7	4.692	1.1368	a8	2.594	0.4129	a9	1.952	0.2506
Commercial Au NRs	a10	4.755	1.3354	a11	3.127	0.5527	a12	2.131	0.2724

acoustic parameters and the wavelength-dependent local light fluence. The difference in oxygen saturation before and after correction was small,[45] so it was set to 1 here. Notably, the calculated C_{HbO_2} and C_{Hb} values are relative due to the unknown coefficient k, while the oxygen saturation (sO_2) value calculated from eqn (1) is absolute.

4 Conclusions

Au NRs with a broad absorption band (650–1100 nm) over the first NIR window were obtained *via* a seed-assistant method in three steps. The prepared Au NRs can be conveniently transferred to the aqueous phase for PEGylation, showing good photostability and low biotoxicity. Owing to the broad absorption band in the NIR region, Au NR@PEG could significantly improve the efficiency of *in vitro* and *in vivo* PAI under multiple excitation wavelengths (532, 680 and 828 nm). Based on this, the synthesized Au NR@PEG could provide a feasible, convenient and efficient means of multifunctional PAI deep in the body, such as for measuring the distribution of oxygen saturation.

Conflicts of interest

There are no conflicts to declare.

Acknowledgements

This work was supported by the National Natural Science Foundation of China (Grant No. 11602159, 51205276, and 61474079), the Special Talents in Shanxi Province (Grant No. 201605D211020), the Scientific & Technological Innovation Programs of Higher Education Institutions in Shanxi (Grant No. 2016136) and the 2018 Study Abroad Program for the University-Sponsored Young Teachers.

Notes and references

1 Y. Jiang and K. Pu, *Small*, 2017, **13**, 1700710.
2 D. Cui, C. Xie, Y. Lyu, X. Zhen and K. Pu, *J. Mater. Chem. B*, 2017, **5**, 4406–4409.
3 X. Wang, Y. Ma, X. Sheng, Y. Wang and H. Xu, *Nano Lett.*, 2018, **18**, 2217–2225.
4 Z. Xu, X. Chen, Y. Jiang, X. Ai, B. Xing and K. Pu, *ACS Nano*, 2018, **18**, 1498–1505.
5 J. T. Robinson, G. Hong, Y. Liang, B. Zhang, O. K. Yaghi and H. Dai, *J. Am. Chem. Soc.*, 2012, **134**, 10664–10669.
6 C. W. Ng, J. Li and K. Pu, *Adv. Funct. Mater.*, 2018, **28**, 1804688.
7 Y. Jiang, J. Li, X. Zhen, C. Xie and K. Pu, *J. Am. Chem. Soc.*, 2019, **141**, 4073–4079.
8 J. Li, J. Huang, J. Huang, Y. Jia, C. Xie and K. Pu, *ACS Nano*, 2018, **12**, 2643–2651.
9 J. Lemaster and J. Jokerst, *Wiley Interdiscip. Rev.: Nanomed. Nanobiotechnol.*, 2017, **9**, e1404.
10 Y. Jiang and K. Pu, *Acc. Chem. Res.*, 2018, **51**, 1840–1849.
11 T. Bao, W. Yin, X. Zheng, X. Zhang, J. Yu, X. Dong, Y. Yong, F. Gao, L. Yan, Z. Gu and Y. Zhao, *Biomaterials*, 2016, **76**, 11–24.
12 Y. Yong, L. Zhou, S. Zhang, L. Yan, Z. Gu, G. Zhang and Y. Zhao, *NPG Asia Mater.*, 2016, **8**, e273.
13 X. Zhen, X. Feng, C. Xie, Y. Zheng and K. Pu, *Biomaterials*, 2017, **127**, 97–106.
14 Q. Chen, C. Wang, C. Liang and Z. Liu, *J. Control. Release*, 2014, **35**, 8206–8214.
15 X. Qian, S. Shen, T. Liu, L. Cheng and Z. Liu, *Nanoscale*, 2015, **7**, 6380–6387.
16 H. Xie, Z. Li, Z. Sun, J. Shao, X.-F. Yu, Z. Guo, J. Wang, Q. Xiao, H. Wang and Q.-Q. Wang, *Small*, 2016, **12**, 4136–4145.
17 Z. Zhou, Y. Sun, J. Shen, J. Wei, C. Yu, B. Kong, W. Liu, H. Yang, S. Yang and W. Wang, *Biomaterials*, 2014, **35**, 7470–7478.
18 X. Zhu, W. Feng, J. Chang, Y.-W. Tan, J. Li, M. Chen, Y. Sun and F. Li, *Nat. Commun.*, 2016, **7**, 10437.
19 S. K. Maji, S. Sreejith, J. Joseph, M. Lin, T. He, Y. Tong, H. Sun, S. W.-K. Yu and Y. Zhao, *Adv. Mater.*, 2014, **26**, 5633–5638.
20 C. Wang, L. Xu, C. Liang, J. Xiang, R. Peng and Z. Liu, *Adv. Mater.*, 2014, **26**, 8154–8162.
21 M. A. Patel, H. Yang, P. L. Chiu, D. D. T. Mastrogiovanni, C. R. Flach, K. Savaram, L. Gomez, A. Hemnarine, R. Mendelsohn and E. Garfunkel, *ACS Nano*, 2013, **7**, 8147–8157.
22 S. Gao, L. Zhang, G. Wang, K. Yang, M. Chen, R. Tian, Q. Ma and L. Zhu, *Biomaterials*, 2016, **79**, 36–45.
23 W. Li and X. Chen, *Nanomedicine*, 2015, **10**, 299–320.
24 H. Ju, R. A. Roy and T. W. Murray, *Biomed. Opt. Express*, 2013, **4**, 66–76.

25 E. Locatelli, I. Monaco and M. Comes Franchini, *RSC Adv.*, 2015, **5**, 21681–21699.
26 Z. Li, H. Huang, S. Tang, Y. Li, X.-F. Yu, H. Wang, P. Li, Z. Sun, H. Zhang, C. Liu and P. K. Chu, *Biomaterials*, 2016, **74**, 144–154.
27 P. Wu, D. Deng, J. Gao and C. Cai, *ACS Appl. Mater. Interfaces*, 2016, **8**, 10243–10252.
28 M. Sun, F. Liu, Y. Zhu, W. Wang, J. Hu, J. Liu, Z. Dai, K. Wang, Y. Wei, J. Bai and W. Gao, *Nanoscale*, 2016, **8**, 4452–4457.
29 M. F. Tsai, S.-H. G. Chang, F.-Y. Cheng, V. Shanmugam, Y.-S. Cheng, C.-H. Su and C.-S. Yeh, *ACS Nano*, 2013, **7**, 5330–5342.
30 I. G. Theodorou, Z. A. R. Jawad, Q. Jiang, E. O. Aboagye, A. E. Porter, M. P. Ryan and F. Xie, *Chem. Mater.*, 2017, **29**, 6916–6926.
31 J. V. Jokerst, A. J. Cole, D. V. D. Sompel and S. S. Gambhir, *ACS Nano*, 2012, **6**, 10366–10377.
32 P. Huang, J. Lin, W. Li, P. Rong, Z. Wang, S. Wang, X. Wang, X. Sun, M. Aronova and G. Niu, *Angew. Chem., Int. Ed.*, 2013, **52**, 13958–13964.
33 S. Mallidi, T. Larson, J. Tam, P. P. Joshi, A. Karpiouk, K. Sokolov and S. Emelianov, *Nano Lett.*, 2009, **9**, 2825–2831.
34 Y. Jiang, P. K. Upputuri, C. Xie, Y. Lyu, L. Zhang, Q. Xiong, M. Pramanik and K. Pu, *Nano Lett.*, 2017, **17**, 4964–4969.
35 H. J. Wang, K. H. Yang, S. C. Hsu and H. Y. Huang, *Nanoscale*, 2016, **8**, 965.
36 Z. L. Zhang, D. W. Pang, Z. Q. Tian, D. L. Zhu, C. N. Zhu and P. Jiang, *ACS Appl. Mater. Interfaces*, 2013, **5**, 1186–1189.
37 D. Wu, J. Yang, G. Zhang and H. Jiang, *Biomed. Opt. Express*, 2017, **8**, 2276–2286.
38 N. R. Jana, L. Gearheart and C. J. Murphy, *J. Phys. Chem. B*, 2001, **105**, 4065–4067.
39 H. Y. Wu, H. C. Chu, T. J. Kuo, C. L. Kuo and M. H. Huang, *Chem. Mater.*, 2005, **17**, 6447–6451.
40 H. Y. Wu, W. L. Huang and M. H. Huang, *Cryst. Growth Des.*, 2009, **7**, 831–835.
41 L. S. Slaughter, W.-S. Chang, P. Swanglap, A. Tcherniak, B. P. Khanal, E. R. Zubarev and S. Link, *J. Phys. Chem. C*, 2010, **114**, 4934–4938.
42 L. Cheng, J. Liu, X. Gu, H. Gong, X. Shi, T. Liu, C. Wang, X. Wang, G. Liu, H. Xing, W. Bu, B. Sun and Z. Liu, *Adv. Mater.*, 2014, **26**, 1886–1893.
43 Z. Li, Y. Hu, M. Chang, K. A. Howard, X. Fan, Y. Sun, F. Besenbacher and M. Yu, *Nanoscale*, 2016, **8**, 16005–16016.
44 C. Kim, C. Favazza and L. V. Wang, *Chem. Rev.*, 2010, **110**, 2756–2782.
45 M. Sivaramakrishnan, K. Maslov, H. F. Zhang, G. Stoica and L. V. Wang, *Phys. Med. Biol.*, 2007, **52**, 1349–1361.